

Oxidation of 2D electrenes: structural transition and the formation of half-metallic channels protected by oxide layers

Pedro H. Souza^{1,*}, Danilo Kuritza^{2,†}, José E. Padilha^{2,‡} and Roberto H. Miwa^{1,§}

¹*Instituto de Física, Universidade Federal de Uberlândia,
C.P. 593, 38400-902, Uberlândia, MG, Brazil and*

²*Campus Avançado Jandaia do Sul,
Universidade Federal do Paraná,
86900-000, Jandaia do Sul, PR, Brazil.*

(Dated: April 6, 2022)

ABSTRACT

Based on first-principles calculations we performed a systematic study of the structural stability, and the electronic properties of oxidized A_2B electrenes. Initially we have considered one-side fully oxidized A_2B single layer electrenes (O/A_2B), with $A = \text{Ba, Ca, Sr, Y}$, and $B = \text{As, N, P, C}$. We show that the hexagonal lattice of the pristine host is no longer the ground state structure in the oxidized systems. Our total energy results reveal an exothermic structural transition from hexagonal to tetragonal ($h \rightarrow t$) geometry, resulting in layered tetragonal structures $[(AOAB)^t]$. Phonon spectra calculations show that the $(AOAB)^t$ systems are dynamically stable for $A = \text{Ba, Ca, Sr}$, and $B = \text{N}$ $[(AOAN)^t]$. In the sequence, we have examined the surface oxidation of bilayer systems $[O/(A_2N)_2/O]$, with $A = \text{Ca, Sr, Ba}$, where we have also found an exothermic $h \rightarrow t$ transition to a dynamically stable layered tetragonal phase $[(AO(AN)_2AO)^t]$. Further electronic structure calculations of reveal the formation of half-metallic bands spreading through the AN layers. These findings indicate that $(AOAN)^t$ and $(AO(AN)_2AO)^t$ are quite interesting platforms for application in spintronics; since the half-metallic channels along the AN and $(AN)_2$ layers (core) are protected against the environment conditions by oxidized AO sheets (cover shells).

I. INTRODUCTION

Research works addressing two-dimensional (2D) materials with different functionalities have been boosted in the last few year. Since the successful synthesis of graphene,¹ 2D materials have been considered as a new paradigm not only in fundamental studies, like the search of topological,²⁻⁴ and tuneable magnetic phases in 2D systems,⁵⁻⁸ but also in technological applications. For instance, addressing the development of new materials for (nano)electronic and spintronic devices like single layer field effect transistors,⁹ and half-metals¹⁰⁻¹⁴ based on transition metal dichalcogenides and dihalides.

By taking advantage of the layered structure of their 3D parents, and a suitable balance between strong (weak) intralayer (interlayer) binding interactions,¹⁵ two dimensional materials can be obtained through exfoliation processes. Indeed, in a seminal work, of Lee *et al.*¹⁶ revealed the exfoliable nature, and the two dimensional electronic confinement in Ca_2N electrides. Electrides are ionic crystals characterized by the presence of electrons not bonded to a particular nucleus. These electrons act as ions (with no nucleus) embedded within the crystal lattice, anionic electrons.^{17,18} Further experimental works

revealed that these anionic electrons form nearly free 2D electron gas confined between the stacked layers of the electride.^{16,19,20} It is worth noting that there are other native inorganic electrides with the same lattice structure of Ca_2N , like Sr_2N ²¹ and Y_2C ;²² meanwhile other ones have been predicted throughout high-throughput computational simulations.^{23,24}

Currently, few layer systems of electrides (electrenes) have attracted research works in fundamental issues, like the search of topological phases throughout the design of kagome lattices on the electrone surface,²⁵ as well as to the development of electronic devices with high carrier density and electronic mobility.^{26,27} Further, theoretical studies have addressed the functionalization of Ca_2N electrenes mediated by atomic adsorption.²⁸ Functionalization is a quite promising route in order to tailor the electronic and magnetic properties of 2D systems. For instance, the rise of ferromagnetic (FM) phases upon full hydrogenation,²⁹ and oxidation of Ca_2N and Sr_2N electrenes.^{30,31} On the other hand, it is important to stress that the presence of anionic electrons makes the electrone surface very reactive, which may lead to significant changes on the electronic and structural properties of the functionalized systems, giving rise to a new set of physical properties to be exploited.

In this work, by means of first-principles calculations, we perform a systematic investigation of the structural stability, and the electronic properties of oxidized electrenes (A_2B), with $A = \text{Ca, Sr, Ba, Y}$, and $B = \text{As, N, P, C}$. Firstly we have considered the full oxidation

* psouza8628@gmail.com

† danilo.kuritza@gmail.com

‡ jose.padilha@ufpr.br

§ hiroki@ufu.br

of one surface side of single layer electrene (O/A_2B). The structural stability was examined through a combination of formation energy results, and phonon spectra calculations. The former indicate an exothermic hexagonal \rightarrow tetragonal structural transition ($h \rightarrow t$); while phonon spectra results reveal that tetragonal phase of O/A_2B [$(AOAB)^t$] is dynamically stable for $B = N$, i.e. $(AOAN)^t$ with $A = Ca, Sr, Ba$, and O/Y_2C . In the sequence, we have considered the surface oxidation of bilayer electrenes, $(A_2N)_2$, with $A = Ca, Sr$ and Ba , where both surfaces sides of were oxidized [$O/(A_2N)_2/O$]. We found a structural transition to the tetragonal phase, which is characterized by $(AN)_2$ layers sandwiched by oxidized AO sheets [$(AO(AN)_2AO)^t$]. Further electronic structure calculations indicate the rise of an energetically stable FM phase, and the emergence of half-metallic band ruled by the in-plane $N-2p_{x,y}$ orbitals, and thus resulting in half-metallic channels along the $(AN)_2$ core shielded by oxidized AO shells.

II. COMPUTATIONAL DETAILS

The calculations were performed by using the density functional theory (DFT),³² as implemented in the computational codes Quantum-Espresso (QE)³³ and Vienna Ab initio Simulation Package (VASP).^{34,35} We have considered the generalized gradient approximation of Perdew-Burke-Ernzerhof (GGA-PBE)³⁶ for the exchange-correlation functional. The single layer and bilayer A_2B electrenes were simulated using slab structures within the supercell approach, with a vacuum region of 18 and 22 Å, respectively, and surface periodicities of (1×1) , and $(\sqrt{2} \times \sqrt{2})$ for hexagonal and tetragonal structures. The final atomic geometries and the total energies were obtained using the QE code, where the Kohn-Sham³⁷ orbitals, and the self-consistent total charge densities were expanded in plane wave basis sets with energy cutoffs of 70 and 353 Ry, respectively. The Brillouin zone sampling was performed by using a $8 \times 8 \times 1$ k-point mesh.³⁸ The atomic positions were relaxed until the residual forces were converged to within 5 meV/Å, and the structural relaxation (variable-cell) was performed within a pressure convergence of 0.05 Kbar. The long-range van der Waals (vdW) interactions were examined using the self-consistent vdW-DF approach.^{39–41}

The electronic structure calculations and structural/thermal stability simulations were performed using the VASP code. We have considered an energy cutoff of 500 eV for the plane wave basis set, and the Brillouin zone was sampled using a $15 \times 15 \times 1$ k-point mesh.³⁸ The structural stability was verified through the calculation of elastic constants and the phonon dispersion using PHONOPY code.⁴²

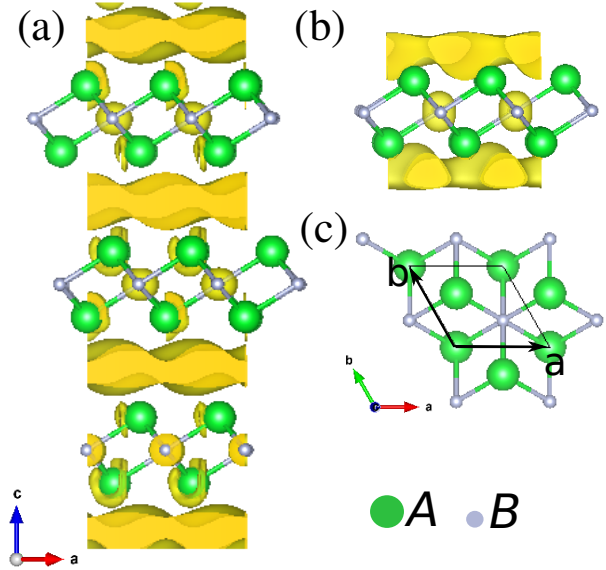


FIG. 1. Structural model of A_2B electride bulk (a), and single layer electrene, side view (b) and top view (c). The isosurfaces (of $0.003 e/\text{\AA}^3$) show the localization of the anionic electrons within the energy interval of ± 0.5 eV with respect to the Fermi level.

III. RESULTS AND DISCUSSIONS

A. Pristine A_2B electrenes

The A_2B electrides with $A = Ca, Sr, Ba, Y$, and $B = N, P, As, C$ share the same structure of Ca_2N , Fig. 1(a). Our results of equilibrium geometries of the A_2B electrides and 2D single layer electrenes, summarized in Table I, are in good agreement with previous experimental and theoretical studies, viz.: Ca_2N ,^{29,30,43,44} Ba_2N ,^{30,45} Ba_2P ,⁴⁶ Sr_2N ,^{21,30} Sr_2P ,⁴⁶ Y_2C ,^{22,47} and Ba_2As .⁴⁶ The mechanical properties of these electrides are anisotropic, characterized by a strong intralayer interactions due to the $A-B$ ionic chemical bonds, and A_2B-A_2B interlayer interactions, which is comparatively weak, with larger interlayer (cation-cation) distance. The latter is ruled by a superposition of (i) Coulombic attractive interactions between the positively charged A_2B layer and the ionic electrons, and (ii) repulsive interaction between the positively charged A_2B layers.^{17,20,26} In order to provide a quantitative picture of the interlayer binding strength [(ii)], we calculate the interlayer binding energy (E^b) defined as,⁴⁸

$$E^b = \frac{1}{S} (E[A_2B]_{ML} - E[A_2B]_{Bulk}),$$

where $E[A_2B]_{ML}$ and $E[A_2B]_{Bulk}$ are the total energies of single layer electrene, and A_2B electride, respectively, and S is the surface area normal to the A_2B stacking. Our results of binding energies for Ca_2N , Sr_2N , Ba_2N , and Y_2C (Table I) are in good agreement with those pre-

TABLE I. Details of the equilibrium geometry of A_2B electrides and single layer electrenes, lattice constant a and $A-B$ equilibrium bond length (in Å), and the interlayer binding energy, E^b (in J/m²) without/with the inclusion of vdW interactions.

A_2B	bulk			monolayer	
	a	$A-B$	E^b	a	$A-B$
Ba ₂ As	4.64	3.21	0.41/0.48	4.65	3.22
Ba ₂ P	4.65	3.18	0.44/0.51	4.64	3.17
Sr ₂ P	4.45	3.01	0.59/0.64	4.43	3.00
Y ₂ C	3.61	2.47	1.60/1.73	3.50	2.45
Ca ₂ N	3.60	2.42	0.97/1.02	3.61	2.43
Sr ₂ N	3.84	2.60	0.78/0.83	3.85	2.61
Ba ₂ N	4.02	2.76	0.58/0.64	4.00	2.75

sented in the current literature.^{18,49}

Given the larger A_2B - A_2B interlayer distance (> 3 Å), it is worth to examine the contribution of the van der Waals (vdW) interactions in the binding energies. As shown in Table I, the calculations of E^b without/with the inclusion of the vdW interactions reveal a slight increase of E^b , for instance between 5 and 10% for the nitrides, A_2N . Thus, we can infer that the Coulombic attractive forces is the main player in the interlayer interactions.

Our results of E^b indicate that these A_2B systems can be classified as “potentially exfoliable” based on the criteria presented by Mounet *et al.* in a recent high-throughput computational investigation applied to two dimensional material.¹⁵ At the equilibrium geometry, the single layer electrene [Figs.1(b) and (c)] exhibits the same A_2B atomic structure of its bulk (electride) parent, with the presence of anionic electrons lying on the electrene surface [Fig. 1(b)].

B. Oxidation

Here we will address the energetic stability and the electronic properties of the oxidized A_2B electrenes. Firstly, we have considered the one sided fully oxidized single layer electrene $[O/(A_2B)]$, and in the sequence the two sided fully oxidized bilayer electrene $[O/(A_2B)_2/O]$. In Figs. 2(a) and (b) we present the structural models of O/A_2B and $O/(A_2B)_2/O$.

1. Structural and Energetic Properties

The energetic stability of O/A_2B was inferred through the calculation of the formation energy (E^f),

$$E^f = E[O/A_2B] - E[A_2B] - E[O_2]/2,$$

where $E[A_2B]$ and $E[O/A_2B]$ are the total energies of pristine and one side fully oxidized electrenes; and $E[O_2]$ is the total energy of an isolated O_2 molecule (triplet state). We found an energetic preference for the oxygen adatoms on the hollow site aligned with the (cation)

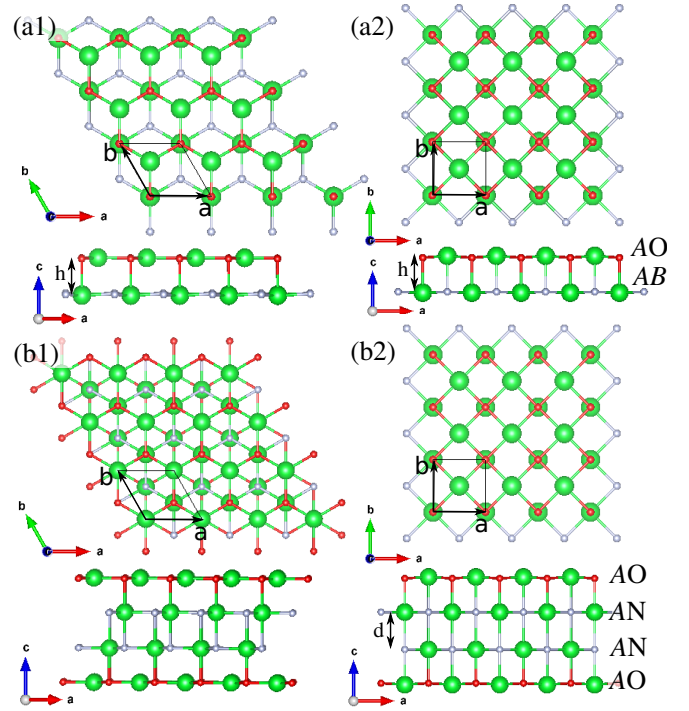


FIG. 2. Structural models of oxidized systems. (a1) Hexagonal and (a2) tetragonal one sided fully oxidized single layer electrene; two sided fully oxidized (b1) hexagonal and (b2) tetragonal bilayer electrene.

A atom at the opposite side of the A_2B monolayer, as shown in Fig. 2(a1). Our results, summarized in Table II, indicate that the oxidation of the A_2B electrenes takes place upon dissociation of the O_2 molecules, $E^f < 0$, where the hexagonal lattice of the A_2B host has been preserved $[O/(A_2B)^h]$. However, further phonon spectra calculations, Fig. 3(a), revealed that the all $O/(A_2B)^h$ structures, except $O/(Y_2C)^h$, present imaginary frequencies, thus indicating that they are dynamically unstable.

In a very recent study,³¹ we found that the hexagonal geometry of one sided oxidized Ca_2N electrene $[O/(Ca_2N)^h]$ is a metastable configuration, which becomes stable through a structural transition to a layered tetragonal phase $[(CaOCaN)^t]$, in Fig. 2(a2)]. In this sense, firstly, we examine if such a $h \rightarrow t$ structural transition is energetically favorable for the other O/A_2B electrenes, and then we will verify the dynamical stabilities of the tetragonal phases by performing a set of phonon spectra calculations. The $h \rightarrow t$ energy gain (ΔE^{h-t}) is given by the total energy difference between the two structural phases, $\Delta E^{h-t} = E^t - E^h$. We found that the tetragonal phases are energetically more stable than the hexagonal ones for all O/A_2B systems of the present study, $\Delta E^{h-t} < 0$. Meanwhile, further phonon spectra calculations revealed that the tetragonal structures become dynamically stable only for $A=N$, $(AOAB)^t$. As shown in Fig. 3(b), the imaginary frequencies present in the hexagonal phase were suppressed in $(CaOCaN)^t$, $(SrOSrN)^t$,

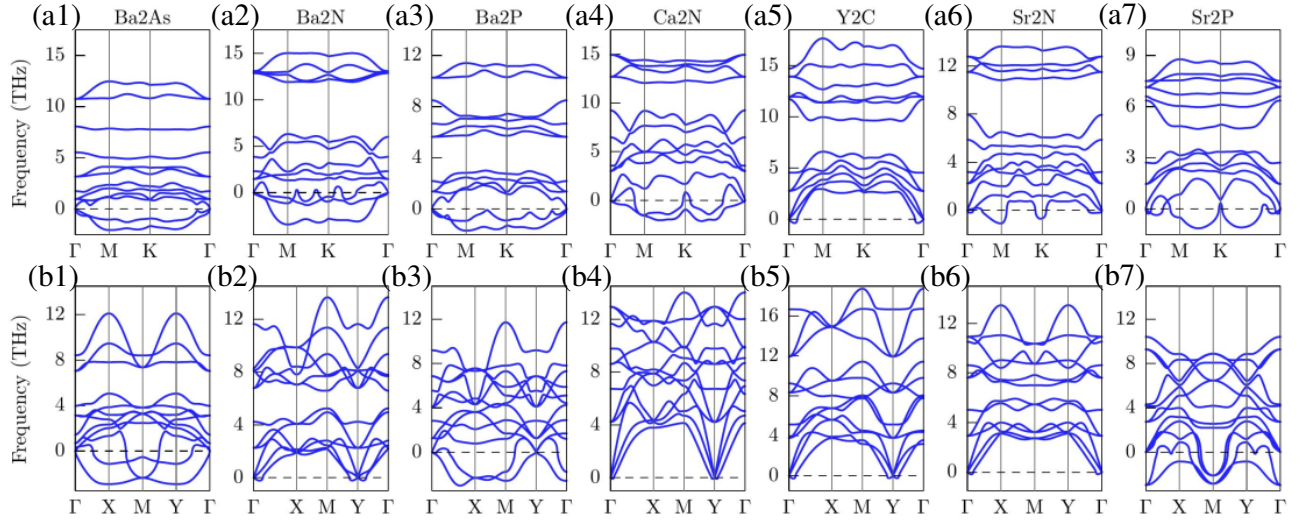


FIG. 3. Phonon spectra of the hexagonal (a) and tetragonal (b) of O/A_2B electrenes.

TABLE II. Oxygen adsorption energy E^{ads} (eV/O-atom), equilibrium lattice constant (a in Å) of the hexagonal (Ox-hexag.) and tetragonal (Ox-tetrag.) fully oxidized A_2B electrenes, O/A_2B , and the total energy gain upon hexagonal \rightarrow tetragonal structural transition in the oxidized systems. The lattice constant of the pristine hexagonal A_2B electrone are within parentheses.

O/A_2B	hexagonal		\rightarrow	tetragonal	
A_2B	E^f	a	$\Delta E^{\text{h-t}}$	a	h
Ba ₂ As	-1.79	4.07 (4.65)	-0.51	3.75	2.80
Ba ₂ P	-2.08	4.42 (4.64)	-0.63	4.18	2.64
Sr ₂ P	-2.21	4.33 (4.43)	-0.76	3.92	2.50
Y ₂ C	-5.46	3.64 (3.50)	-0.20	3.40	2.58
Ca ₂ N	-2.99	3.85 (3.61)	-0.90	3.36	2.40
Sr ₂ N	-3.00	4.11 (3.85)	-0.80	3.59	2.54
Ba ₂ N	-3.08	4.35 (4.00)	-0.57	3.83	2.61
$O/(A_2B)_2/O$	hexagonal		\rightarrow	tetragonal	
A_2B	E^f	a	$\Delta E^{\text{h-t}}$	a	d
Ca ₂ N	-3.04	3.92	-1.68	3.40	2.57
Sr ₂ N	-3.07	4.19	-1.27	3.63	2.85
Ba ₂ N	-3.02	4.33	-1.10	3.86	3.22

and (BaOBaN)^t.

In the sequence, we have considered the surface oxidation of bilayer A_2B electrenes with $A = \text{N}$, $O/(A_2\text{N})_2/O$ [Fig. 2(b)]. Similarly to what we have found for the single layer systems, the $O/(A_2\text{N})_2/O$ systems are (i) energetically ($E^f < 0$ in Table II), and also (ii) present exothermic $\text{h} \rightarrow \text{t}$ structural transitions, with $\Delta E^{\text{h-t}}$ almost twice compared with those of the O/A_2B counterparts.

The tetragonal phase of the oxidized electrenes, (AOAN)^t, and (AO(AN)₂AO)^t, with $A = \text{Ba, Ca, Sr}$, can be characterized by parallel sheets indicated as OA and NA in Figs. 2(a2) and (b2). Interestingly, the energetic preference for the tetragonal phase, $\Delta E^{\text{h-t}} < 0$, can be discussed/justified in light of the stoichiometrically

equivalent OA and NA bulk cubic parents for $A = \text{Ca, Sr, Ba}$, that is, CaO, SrO, and BaO,^{50–53} and CaN, SrN, and BaN.⁵³ The former present zero energy above the hull⁵⁴ ($\Delta E^{\text{hull}} = 0$), while in the latter we have $\Delta E^{\text{hull}} = 0.43, 0.52, 0.40$ eV/atom, with equilibrium lattice constants differing by about 6% when compared with those of the oxidized (AOAN)^t and (AO(AN)₂AO)^t systems.

2. Electronic and Magnetic Properties

The electronic band structures of the A_2B electrenes, with $A = \text{Ca, Sr, Ba}$, and $B = \text{N}$ are characterized by parabolic metallic bands, giving rise to nearly free electron (NFE) states localized on the electrone's surface and between the stacked layers. On the other hand, upon the formation of AO oxidized layers these NFE states become unoccupied, and we observe the emergence of magnetic moments on the AN layers. Here, we will examine on the magnetic and electronic properties of energetically and structurally stable oxidized electrenes, (AOAN)^t and (AO(AN)₂AO)^t.

Based on the nominal oxidation states and the electronegativities of the involved atoms, we can infer the emergence of a magnetic moment in the oxidized systems.³⁰ There is a net charge transfer of 2 electrons from each (less electronegative) A atoms to the (more electronegative) O and N atoms, resulting in A^{2+} , O^{2-} and N^{2-} oxidation states, Fig. 4(a). The ground state configuration is characterized by a OA (oxidized) layers with closed p shells parallel to a AN layer with the N-2p orbitals partially occupied. According to the Hund's rule, each N atom will carry a net magnetic moment of $1 \mu_B$. Indeed, within the GGA-PBE approach, we found a net magnetic moment of about $0.8 \mu_B$ per formula unit, mostly localized on the nitrogen atoms. The electronic

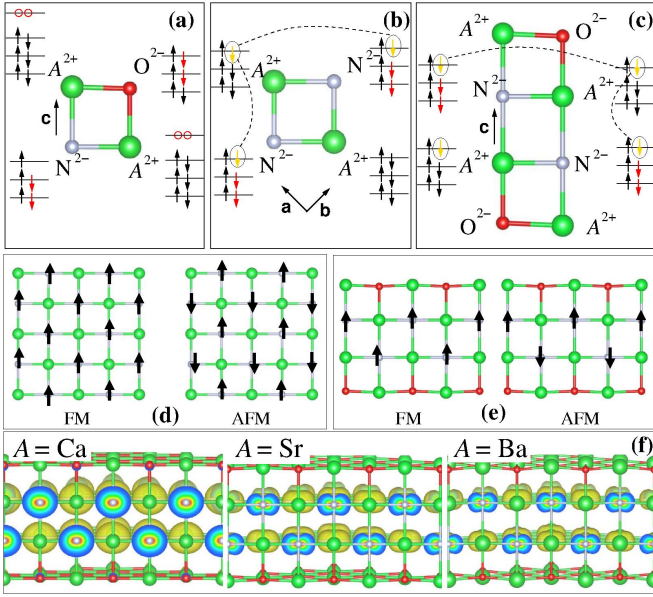


FIG. 4. Schematic orbital occupation of $(\text{AOAN})^t$ (a) AO and NO layers along the stacking direction (c), and (b) NA sheet perpendicular to the stacking direction, $\mathbf{a} \times \mathbf{b}$ plane. (c) Orbital occupation of $(\text{AO}(\text{AN})_2\text{AO})^t$ along the stacking direction. (d) Intralayer and (e) interlayer FM/AFM spin-polarizations. (f) Spin-density distribution of the $(\text{AO}(\text{AN})_2\text{AO})^t$ systems. Isosurface of $0.004 \text{ e}/\text{\AA}^2$.

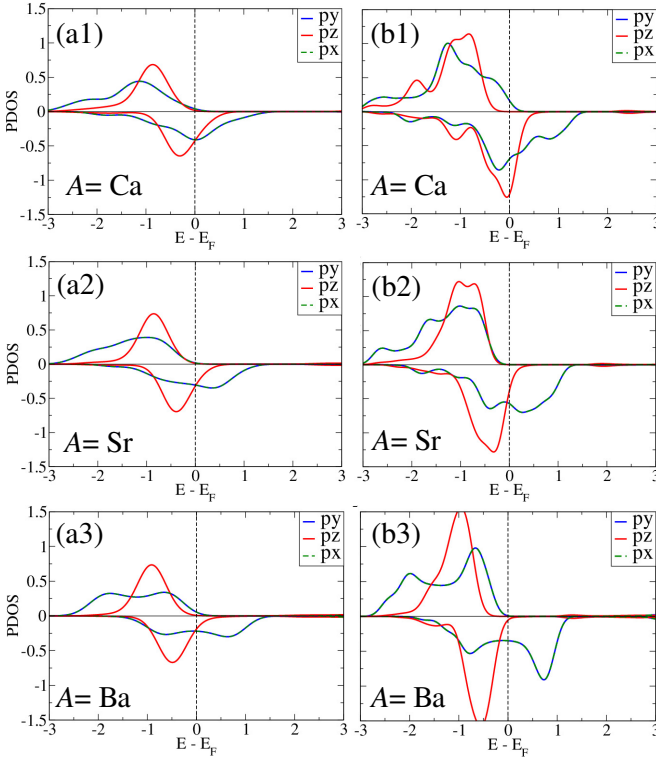


FIG. 5. Electronic density of states (DOS) projected on the N-2p orbitals of $(\text{AOAN})^t$ (a1)-(a3), $(\text{AO}(\text{AN})_2\text{AO})^t$ (b1)-(b3).

density of states (DOS) projected on the N-2p orbitals of $(\text{AOAN})^t$ and $(\text{AO}(\text{AN})_2\text{AO})^t$, Figs. 5(a) and (b), reveal that the partial occupation of planar N-2 $p_{x,y}$ orbitals brings the major contribution to the polarization of the N atoms.

Further total energy comparisons between the magnetic and non-magnetic phases, $\Delta E^{\text{mag}} = E^{\text{mag}} - E^{\text{non-mag}}$ support the energetic preference for the spin-polarization systems, $\Delta E^{\text{mag}} < 0$ in Table III. The strength of the magnetic interactions between the nitrogen atoms was examined by comparing the total energies of the ferromagnetic (FM) and antiferromagnetic (AFM) phases as shown in Fig. 4(d) and (e). We have considered intralayer interactions ($\Delta E_{\text{intra}}^{\text{FM-AFM}}$) between the N atoms in the same AN layer [Fig. 4(d)], and interlayer interactions ($\Delta E_{\text{inter}}^{\text{FM-AFM}}$) between the N atoms lying in different layers [Fig. 4(e)] in the case of $(\text{AO}(\text{AN})_2\text{AO})^t$. Our results, summarized in Table III, reveal the both systems, $(\text{AOAB})^t$ and $(\text{AO}(\text{AB})_2\text{AO})^t$, present an energetic preference for the intralayer and interlayer FM coupling between the N atoms. It is noticeable that (i) $(\text{CaO}(\text{CaN})_2\text{CaO})^t$ presents the largest interlayer FM interaction, $\Delta E_{\text{inter}}^{\text{FM-AFM}} = 36.5 \text{ meV/N-atom}$, compared with the other $(\text{AO}(\text{AN})_2\text{AO})^t$ systems, leading to (ii) a strengthening of the intralayer FM coupling, namely $\Delta E_{\text{intra}}^{\text{FM-AFM}} = 8.5 \rightarrow 22.8 \text{ meV/N-atom}$. In contrast, (iii) we found (relatively) lower values of $\Delta E_{\text{inter}}^{\text{FM-AFM}}$ for $(\text{SrO}(\text{SrN})_2\text{SrO})^t$ and $(\text{BaO}(\text{BaN})_2\text{BaO})^t$ can be due to the larger interlayer distance (d) as indicated in Fig. 2(b2) and Table II, and the more localized feature of the spin-polarized states normal to the stacking direction (c). Indeed, the projection of the DOS on the N- p_z orbitals [Fig. 5(b)] support the larger interlayer interaction in $(\text{CaO}(\text{CaN})_2\text{CaO})^t$ [Fig. 5(b1)] compared with those of other oxidized bilayer electrenes, Figs. 5(b2) and (b3).

The energetic preference for the FM phase can be attributed to super-exchange interactions between the N^{2+} anions mediated by A^{2+} cations. In this sense, the FM coupling will be favored due to the electron delocalization along the $\text{N}^{2+}-\text{A}^{2+}-\text{N}^{2+}$ bonds, thus lowering the kinetic energy of the system, as schematically shown in Figs. 4(b) and (c) for the intralayer and interlayer couplings, respectively. Further support to the FM coupling between the N^{2+} anions, mediated by super-exchange interactions, can be found in the Goodenough-Kanamori rule,^{55,56} since the $\text{N}^{2+}-\text{A}^{2+}-\text{N}^{2+}$ bonds are characterized by bond angles of 90° . In Fig. 4(f) we present the spin-density distribution in $(\text{AO}(\text{AB})_2\text{AO})^t$, with $\text{A}=\text{Ca}$, Sr , Ba , respectively, where we confirm the localization of the net magnetic moment on the nitrogen atoms.

In Fig. 6 we present the electronic band structures and the projection of the electronic states within an energy interval of $\pm 0.1 \text{ eV}$ with respect to the Fermi level ($E_F \pm 0.1 \text{ eV}$). The single layer $(\text{AOAN})^t$ systems, with $\text{A}=\text{Ca}$, Sr , and Ba [Fig. 6(a1)-(c1)] share similar electronic features, namely (i) fully unoccupied NFE parabolic bands lying between 1 and 2 eV above E_F , with the (NFE) orbitals spreading out on the oxidized surface

TABLE III. Total energy differences in meV/N-atom. * = from our previous paper.

	ΔE^{mag}	$\Delta E_{\text{intra}}^{\text{FM-AF}}$	$\Delta E_{\text{inter}}^{\text{FM-AF}}$
$(\text{CaOCaN})^t$	67	8.5	—
$(\text{SrOSrN})^t$	135	18.7	—
$(\text{BaOBaN})^t$	92	1.9	—
$(\text{CaO}(\text{CaN})_2\text{CaO})^t$	83	22.8	36.5
$(\text{SrO}(\text{SrN})_2\text{SrO})^t$	127	12.9	1.0
$(\text{BaO}(\text{BaN})_2\text{BaO})^t$	93	4.4	0.5

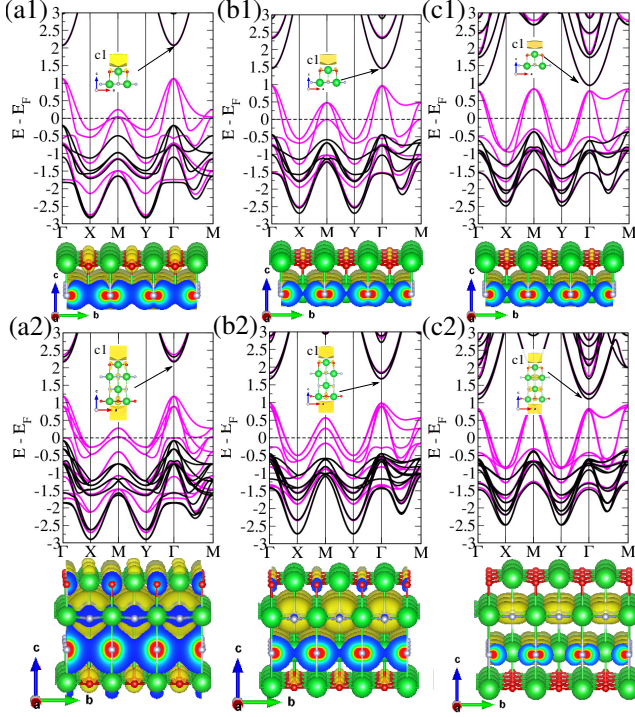


FIG. 6. Electronic band structure and the electron distribution near the Fermi level ($E_F \pm 0.1$ eV) of $(\text{AOAN})^t$, (a1) $(\text{CaOCaN})^t$ (a2) $(\text{SrOSrN})^t$, and (a3) $(\text{BaOBaN})^t$; and $(\text{AO}(\text{AN})_2\text{AO})^t$, (b1) $(\text{CaO}(\text{CaN})_2\text{CaO})^t$ (b2) $(\text{SrO}(\text{SrN})_2\text{SrO})^t$, and (b3) $(\text{BaO}(\text{BaN})_2\text{BaO})^t$. Electronic distribution of the NFE state at the Γ -point (inset). isolated of $0.002 e/\text{\AA}^2$.

(OA) [insets of Figs. 6(a1)-(c1)]; and (ii) the formation of half-metallic bands which are (iii) projected mostly on

the N-2p orbitals. We found somewhat similar electronic properties [(i)-(iii)] in $(\text{AO}(\text{AB})_2\text{AO})^t$, Figs. 6(a2)-(c2), with the NFE states lying on the (both) oxidized AO surfaces (insets). It is worth noting that the projection of the electronic state near the Fermi level ($E_F \pm 0.1$ eV) reveal the formation of half-metallic channels spreading out mostly through the AN (inner layers) which, in its turn, are sandwiched by oxidized AO sheets. That is, the external oxidized layers (AO) act as a shield protecting the (inner) half-metallic channels against the environment conditions. These findings suggest that the oxidized $(\text{AOAN})^t$, and $(\text{AO}(\text{AN})_2\text{AO})^t$ electrenes are interesting materials for application in the development of spintronic devices based on 2D platforms.

IV. SUMMARY AND CONCLUSIONS

By means of first-principles DFT calculations, we have performed a theoretical study of the oxidized 2D single layer $\text{O}/\text{A}_2\text{B}$ and bilayer $[\text{O}/(\text{A}_2\text{B})_2/\text{O}]$ electrenes, with with $A = \text{Ba}, \text{Ca}, \text{Sr}, \text{Y}$, and $B = \text{As}, \text{N}, \text{P}, \text{C}$. We found that $\text{O}/\text{A}_2\text{B}$ and $\text{O}/(\text{A}_2\text{B})_2/\text{O}$ systems with $B = \text{N}$ become stable upon an hexagonal \rightarrow tetragonal structural transition, resulting in layered tetragonal nitride systems, $(\text{AOAN})^t$ and $(\text{AO}(\text{AN})_2\text{AO})^t$, for $A = \text{Ca}, \text{Sr}, \text{Ba}$. We found the emergence of a ferromagnetic phase, with the net magnetic moment mostly ruled by the planar N-2 $p_{x,y}$ orbitals. Further electronic structure calculations reveal the formation of half-metallic bands spreading out through the AN layers, with nearly negligible contribution from the oxidized AO sheets. These results reveal that $(\text{AO}(\text{AN})_2\text{AO})^t$ is a quite interesting core-shell platform for spin-polarized transport on 2D systems, characterized by half-metallic channels lying on the $(\text{AN})_2$ layers (core) protected against the environment conditions by the oxidized AO sheets (shell).

ACKNOWLEDGMENTS

The authors acknowledge financial support from the Brazilian agencies CNPq, CAPES, and FAPEMIG, and the CENAPAD-SP and Laboratório Nacional de Computação Científica (LNCC-SCAFMat2) for computer time.

- [1] K. S. Novoselov, A. K. Geim, S. V. Morozov, D. Jiang, Y. Zhang, S. V. Dubonos, I. V. Grigorieva, and A. A. Firsov, “Electric field effect in atomically thin carbon films,” *science*, vol. 306, no. 5696, pp. 666–669, 2004.
- [2] C. L. Kane and E. J. Mele, “ Z_2 topological order and the quantum spin hall effect,” *Phys. Rev. Lett.*, vol. 95, p. 146802, 2005.
- [3] C. Weeks, J. Hu, J. Alicea, M. Franz, and R. Wu, “Engineering a robust quantum spin hall state in graphene

via adatom deposition,” *Physical Review X*, vol. 1, no. 2, p. 021001, 2011.

- [4] C. M. Acosta, M. P. Lima, R. Miwa, A. J. da Silva, and A. Fazzio, “Topological phases in triangular lattices of ru adsorbed on graphene: ab initio calculations,” *Physical Review B*, vol. 89, no. 15, p. 155438, 2014.
- [5] T. Song, Z. Fei, M. Yankowitz, Z. Lin, Q. Jiang, K. Hwangbo, Q. Zhang, B. Sun, T. Taniguchi, K. Watanabe, *et al.*, “Switching 2d magnetic states via pres-

- sure tuning of layer stacking,” *Nature materials*, vol. 18, no. 12, pp. 1298–1302, 2019.
- [6] T. Li, S. Jiang, N. Sivadas, Z. Wang, Y. Xu, D. Weber, J. E. Goldberger, K. Watanabe, T. Taniguchi, C. J. Fennie, *et al.*, “Pressure-controlled interlayer magnetism in atomically thin CrI_3 ,” *Nature materials*, vol. 18, no. 12, pp. 1303–1308, 2019.
 - [7] E. S. Morell, A. León, R. H. Miwa, and P. Vargas, “Control of magnetism in bilayer CrI_3 by an external electric field,” *2D Materials*, vol. 6, no. 2, p. 025020, 2019.
 - [8] P. d. A. Dominike, I. S. de Oliveira, J. B. Oliveira, W. L. Scopel, and R. H. Miwa, “Magnetic switch and electronic properties in chromium-intercalated two-dimensional GeP_3 ,” *Physical Review Materials*, vol. 5, no. 5, p. 054002, 2021.
 - [9] B. Radisavljevic, A. Radenovic, J. Brivio, i. V. Giacometti, and A. Kis, “Single-layer MoS_2 transistors,” *Nature Nanotechnology*, vol. 6, no. 3, pp. 147–150, 2011.
 - [10] Y. Tong, Y. Guo, K. Mu, H. Shan, J. Dai, Y. Liu, Z. Sun, A. Zhao, X. C. Zeng, C. Wu, *et al.*, “Half-metallic behavior in 2d transition metal dichalcogenides nanosheets by dual-native-defects engineering,” *Advanced Materials*, vol. 29, no. 40, p. 1703123, 2017.
 - [11] V. V. Kulish and W. Huang, “Single-layer metal halides MX_2 ($\text{X} = \text{Cl}, \text{Br}, \text{I}$): stability and tunable magnetism from first principles and monte carlo simulations,” *Journal of Materials Chemistry C*, vol. 5, no. 34, pp. 8734–8741, 2017.
 - [12] G. Gökoğlu and E. Aktürk, “Half metallicity and pressure-induced electronic structure of monolayer FeX_2 ($\text{X} = \text{S}, \text{Se}$),” *Materials Research Express*, vol. 4, no. 11, p. 116305, 2017.
 - [13] Y. Feng, X. Wu, J. Han, and G. Gao, “Robust half-metallicities and perfect spin transport properties in 2d transition metal dichlorides,” *Journal of Materials Chemistry C*, vol. 6, no. 15, pp. 4087–4094, 2018.
 - [14] B. Wang, Q. Wu, Y. Zhang, Y. Guo, X. Zhang, Q. Zhou, S. Dong, and J. Wang, “High curie-temperature intrinsic ferromagnetism and hole doping-induced half-metallicity in two-dimensional scandium chlorine monolayers,” *Nanoscale horizons*, vol. 3, no. 5, pp. 551–555, 2018.
 - [15] N. Mounet, M. Gibertini, P. Schwaller, D. Campi, A. Merkys, A. Marrazzo, T. Sohier, I. E. Castelli, A. Cepellotti, G. Pizzi, *et al.*, “Two-dimensional materials from high-throughput computational exfoliation of experimentally known compounds,” *Nature Nanotechnology*, vol. 13, no. 3, pp. 246–252, 2018.
 - [16] K. Lee, S. W. Kim, Y. Toda, S. Matsuishi, and H. Hosono, “Dicalcium nitride as a two-dimensional electride with an anionic electron layer,” *Nature*, vol. 494, no. 7437, pp. 336–340, 2013.
 - [17] D. L. Druffel, A. H. Woomer, K. L. Kuntz, J. T. Pawlik, and S. C. Warren, “Electrons on the surface of 2d materials: from layered electrides to 2d electrenes,” *Journal of Materials Chemistry C*, vol. 5, no. 43, pp. 11196–11213, 2017.
 - [18] S. Liu, W. Li, S. W. Kim, and J.-H. Choi, “Decisive role of interlayer ionic couplings for the electronic properties of two-dimensional layered electrides,” *The Journal of Physical Chemistry C*, vol. 124, no. 2, p. 1398, 2020.
 - [19] J. S. Oh, C.-J. Kang, Y. J. Kim, S. Sinn, M. Han, Y. J. Chang, B.-G. Park, S. W. Kim, B. I. Min, H.-D. Kim, *et al.*, “Evidence for anionic excess electrons in a quasi-two-dimensional Ca_2N electride by angle-resolved photoemission spectroscopy,” *Journal of the American Chemical Society*, vol. 138, no. 8, pp. 2496–2499, 2016.
 - [20] D. L. Druffel, K. L. Kuntz, A. H. Woomer, F. M. Alcorn, J. Hu, C. L. Donley, and S. C. Warren, “Experimental demonstration of an electride as a 2d material,” *Journal of the American Chemical Society*, vol. 138, no. 49, pp. 16089–16094, 2016.
 - [21] N. E. Brese and M. O’Keeffe, “Synthesis, crystal structure, and physical properties of Sr_2N ,” *Journal of Solid State Chemistry*, vol. 87, no. 1, pp. 134–140, 1990.
 - [22] X. Zhang, Z. Xiao, H. Lei, Y. Toda, S. Matsuishi, T. Kamiya, S. Ueda, and H. Hosono, “Two-dimensional transition-metal electride Y_2C ,” *Chemistry of Materials*, vol. 26, no. 22, pp. 6638–6643, 2014.
 - [23] T. Tada, S. Takemoto, S. Matsuishi, and H. Hosono, “High-throughput ab initio screening for two-dimensional electride materials,” *Inorganic chemistry*, vol. 53, no. 19, pp. 10347–10358, 2014.
 - [24] T. Inoshita, S. Jeong, N. Hamada, and H. Hosono, “Exploration for two-dimensional electrides via database screening and ab initio calculation,” *Physical Review X*, vol. 4, no. 3, p. 031023, 2014.
 - [25] S. Zhang, M. Kang, H. Huang, W. Jiang, X. Ni, L. Kang, S. Zhang, H. Xu, Z. Liu, and F. Liu, “Kagome bands disguised in a coloring-triangle lattice,” *Physical Review B*, vol. 99, no. 10, p. 100404, 2019.
 - [26] S. Zhao, Z. Li, and J. Yang, “Obtaining two-dimensional electron gas in free space without resorting to electron doping: an electride based design,” *Journal of the American Chemical Society*, vol. 136, no. 38, pp. 13313–13318, 2014.
 - [27] X. Zeng, S. Zhao, Z. Li, and J. Yang, “Electron-phonon interaction in a Ca_2N monolayer: Intrinsic mobility of electrene,” *Physical Review B*, vol. 98, no. 15, p. 155443, 2018.
 - [28] L. Liu and H. L. Zhuang, “High-throughput functionalization of single-layer electride Ca_2N ,” *Mater. Res. Express*, vol. 5, p. 076306, 2018.
 - [29] X.-L. Qiu, J.-F. Zhang, Z.-Y. Lu, and K. Liu, “Manipulating the electronic and magnetic properties of monolayer electride Ca_2N by hydrogenation,” *The Journal of Physical Chemistry C*, vol. 123, no. 40, pp. 24698–24704, 2019.
 - [30] C.-W. Wu and D.-X. Yao, “Intriguing p-orbital magnetic semiconductors and carrier induced half-metallicity in surface oxygen-functionalized two-dimensional X_2N ($\text{X} = \text{Ca}, \text{Sr}$) crystals,” *Journal of Magnetism and Magnetic Materials*, vol. 493, p. 165727, 2020.
 - [31] P. H. Souza, J. E. Padilha, and R. H. Miwa, “Structural transition in oxidized Ca_2N electrenes: CaO/Ca 2d heterostructures,” *The Journal of Physical Chemistry C*, vol. 124, no. 27, pp. 14706–14712, 2020.
 - [32] P. Hohenberg and W. Kohn, “Inhomogeneous electron gas,” *Physical review*, vol. 136, no. 3B, p. B864, 1964.
 - [33] P. Giannozzi, S. Baroni, N. Bonini, M. Calandra, R. Car, C. Cavazzoni, D. Ceresoli, G. L. Chiarotti, M. Cococcioni, I. Dabo, *et al.*, “Quantum espresso: a modular and open-source software project for quantum simulations of materials,” *Journal of physics: Condensed matter*, vol. 21, no. 39, p. 395502, 2009.
 - [34] G. Kresse and J. Furthmüller, “Efficiency of ab-initio total energy calculations for metals and semiconductors using a plane-wave basis set,” *Computational materials sci-*

- ence, vol. 6, no. 1, pp. 15–50, 1996.
- [35] G. Kresse and J. Furthmüller, “Efficient iterative schemes for ab initio total-energy calculations using a plane-wave basis set,” *Physical review B*, vol. 54, no. 16, p. 11169, 1996.
 - [36] J. P. Perdew, K. Burke, and M. Ernzerhof, “Generalized gradient approximation made simple,” *Physical review letters*, vol. 77, no. 18, p. 3865, 1996.
 - [37] W. Kohn and L. J. Sham, “Self-consistent equations including exchange and correlation effects,” *Physical review*, vol. 140, no. 4A, p. A1133, 1965.
 - [38] H. J. Monkhorst and J. D. Pack, “Special points for brillouin-zone integrations,” *Physical review B*, vol. 13, no. 12, p. 5188, 1976.
 - [39] M. Dion, H. Rydberg, E. Schröder, D. C. Langreth, and B. I. Lundqvist *Phys. Rev. Lett.*, vol. 92, p. 246401, 2004.
 - [40] G. Roman-Perez and J. M. Soler *Phys. Rev. Lett.*, vol. 103, p. 096102, 2009.
 - [41] J. Klimeš, D. R. Bowler, and A. Michaelides, “Van der waals density functionals applied to solids,” *Physical Review B*, vol. 83, no. 19, p. 195131, 2011.
 - [42] A. Togo and I. Tanaka, “First principles phonon calculations in materials science,” *Scripta Materialia*, vol. 108, pp. 1–5, 2015.
 - [43] D. H. Gregory, A. Bowman, C. F. Baker, and D. P. Weston, “Dicalcium nitride, Ca_2N —a 2d” excess electron” compound; synthetic routes and crystal chemistryelectronic supplementary information (esi) available: Xrd and polaris neutron diffraction refinements. see <http://www.rsc.org/suppdata/jm/b0/b001911i>,” *Journal of Materials Chemistry*, vol. 10, no. 7, pp. 1635–1641, 2000.
 - [44] J. Wang, L. Li, Z. Shen, P. Guo, M. Li, B. Zhao, L. Fang, and L. Yang, “Ultralow interlayer friction of layered electride Ca_2N : A potential two-dimensional solid lubricant material,” *Materials*, vol. 11, no. 12, p. 2462, 2018.
 - [45] O. Reckeweg and F. DiSalvo, “Crystal structure of dibarium mononitride, Ba_2N , an alkaline earth metal subnitride,” *Zeitschrift für Kristallographie-New Crystal Structures*, vol. 220, no. 4, pp. 519–520, 2005.
 - [46] W. Ming, M. Yoon, M.-H. Du, K. Lee, and S. W. Kim, “First-principles prediction of thermodynamically stable two-dimensional electrides,” *Journal of the American Chemical Society*, vol. 138, no. 47, pp. 15336–15344, 2016.
 - [47] J. Hou, K. Tu, and Z. Chen, “Two-dimensional y_2c electride: a promising anode material for na-ion batteries,” *The Journal of Physical Chemistry C*, vol. 120, no. 33, pp. 18473–18478, 2016.
 - [48] J. H. Jung, C.-H. Park, and J. Ihm, “A rigorous method of calculating exfoliation energies from first principles,” *Nano letters*, vol. 18, no. 5, pp. 2759–2765, 2018.
 - [49] S. G. Dale and E. R. Johnson, “The ionic versus metallic nature of 2d electrides: a density-functional description,” *Physical Chemistry Chemical Physics*, vol. 19, no. 40, pp. 27343–27352, 2017.
 - [50] M. Dadsetani and R. Beiranvand, “Optical properties of alkaline-earth metal oxides from first principles,” *Solid state sciences*, vol. 11, no. 12, pp. 2099–2105, 2009.
 - [51] H. Nejatipour and M. Dadsetani, “Excitonic effects in the optical properties of alkaline earth chalcogenides from first-principles calculations,” *Physica Scripta*, vol. 90, no. 8, p. 085802, 2015.
 - [52] D. K. Nguyen, V. Van On, D. Hoat, J. Rivas-Silva, and G. H. Cocoletzi, “Structural, electronic, magnetic and optical properties of cao induced by oxygen incorporation effects: A first-principles study,” *Physics Letters A*, vol. 397, p. 127241, 2021.
 - [53] A. Jain, S. P. Ong, G. Hautier, W. Chen, W. D. Richards, S. Dacek, S. Cholia, D. Gunter, D. Skinner, G. Ceder, and K. a. Persson, “Commentary: The Materials Project: A materials genome approach to accelerating materials innovation,” *APL Materials*, vol. 1, no. 1, p. 011002, 2013.
 - [54] W. Sun, C. J. Bartel, E. Arca, S. R. Bauers, B. Matthews, B. Orvañanos, B.-R. Chen, M. F. Toney, L. T. Schelhas, W. Tumas, *et al.*, “A map of the inorganic ternary metal nitrides,” *Nature materials*, vol. 18, no. 7, pp. 732–739, 2019.
 - [55] J. B. Goodenough, “Theory of the role of covalence in the perovskite-type manganites $[\text{La, m (ii)}] \text{MnO}_3$,” *Physical Review*, vol. 100, no. 2, p. 564, 1955.
 - [56] J. Kanamori, “Crystal distortion in magnetic compounds,” *Journal of Applied Physics*, vol. 31, no. 5, pp. S14–S23, 1960.